Kinetically Controlled Self-Assembly of Phosphorescent Au^{III} Aggregates and Ligand-to-Metal-Metal Charge Transfer Excited State: A Combined Spectroscopic and DFT/TDDFT Study

Qingyun Wan,[†] Jiuxu Xia,[‡] Wei Lu,[‡] Jun Yang,[†] and Chi-Ming Che[†, §, *]

[†]Department of Chemistry and State Key Laboratory of Synthetic Chemistry, The University of Hong Kong, Pokfulam Road, Hong Kong, China

[‡]Department of Chemistry, Southern University of Science and Technology, Shenzhen, Guangdong 518055, China

[§]HKU Shenzhen Institute of Research & Innovation, Shenzhen, China

ABSTRACT: Metallophilic interactions in d^{10}-d^{10}(Au^{I}-Au^{I})/d^{8}-d^{8}(Pt^{II}-Pt^{II}, Rh^{I}-Rh^{I}, Ir^{I}-Ir^{I}) complexes have been widely studied for decades, and metal-metal (M-M) bonding character has been revealed in both the ground and excited states. These M-M closed-shell interactions are appealing driving forces for the self-assembly of supramolecular/polymeric systems, providing luminescent properties distinctly different from those of the corresponding monomer. However, reports on attractive interactions between two Au^{III} complex cations are scarce in the literature. Herein is described a series of pincer-type cationic Au^{III} complexes with different auxiliary ligands, among which the Au^{III}-allenylidene complex displays a close Au-Au contact of 3.367 Å between neighboring molecules in its X-ray crystal structure; Au^{III}-isocyanide complexes show a broad redshifted absorption band and prominent phosphorescence upon aggregation that was influenced by an attractive Au^{III}-Au^{III} bonding interaction in the excited state; and Au^{III}-acetylene complexes can undergo living supramolecular polymerization upon varying the counteranion. The nature of the emissive excited state(s) of the Au^{III} aggregates is assigned to a mixture of major $^{3}[\pi-\pi^{*}]$ and minor ^{3}LMMCT (ligand-to-metal-metal charge transfer) states based on combined spectroscopic and DFT/TDDFT studies. The morphology of the Au^{III} aggregates is highly dependent on the concentration and nature of the counteranion. A qualitative model has been applied to account for the concentration- and counteranion-dependent kinetics of the supramolecular polymerization process.

Introduction

Aurophilic attraction, commonly referred to Au^{I}-Au^{I} interaction, has been subjected to extensive experimental and theoretical studies for decades.[1,2] Pioneering works on Au^{I} systems[2,3] by Pyykkö and coworkers suggest that aurophilic attraction arises mainly from dispersion and virtual charge transfer interactions. In contrast to aurophilicity in Au^{I} chemistry and d^{10}-d^{10} interactions,[2,4-7] investigations on d^{8}-d^{8} Au^{III}-Au^{III} interactions are sparse.[8,9] Whether Au^{III} complexes would display specific low energy electronic transitions upon aggregation, similar to their isoelectronic Pt^{II} and Pd^{II} counterparts, also remains an unanswered question. For decades, square planar Pt^{II} complexes have been widely studied with regard to aspects related to $^{1/3}$MMLCT excited states, supramolecular self-assembly, and photoluminescence, all of which are impacted by the presence of closed-shell Pt^{II}-Pt^{II} interactions.[10-15] Recent studies showed that Pd^{II} complexes can also display Pd^{II}-Pd^{II} interactions and $^{1/3}$MMLCT excited states upon aggregation.[16,17] A series of photoresponsive semiconductors and sensors based on pincer-type Pt^{II} complexes could also be fabricated.[10,18-20] As Au^{III} ion has a higher redox potential and is more electrophilic than Pt^{II} ion, supramolecular materials with new functions could be obtained through a self-assembly process using Au^{III} complexes as building blocks.

Recently, kinetically controlled supramolecular polymerization of cationic Pt^{II} and Pd^{II} complexes has been achieved by modulating the pathway complexity.[21,22] Besenius and coworkers reported the stepwise self-assembly of Au^{I}-metallopeptides in water by making use of Au^{I}-Au^{I} interactions.[23] However, to the best of our knowledge, pincer Au^{III} complexes that undergo a kinetically controlled supramolecular polymerization process are unprecedented, and the excited states of Au^{III} aggregates are scarcely studied.

Kinetic control over supramolecular polymerization, which is also very ubiquitous in the synthesis of biological structures, has been found to be a powerful tool in preparing highly ordered nanostructures with tailored and specific functions.[24-31] An appropriate kinetic energy barrier is the key factor for molecules undergoing a supramolecular polymerization process out of their thermodynamic equilibrium.[32] Seeded supramolecular polymerization can be achieved by manipulating the pathway complexity; however, until recently, only limited studies in this area have been reported.[21,24,26,27,32-42]

Herein, compelling evidence that the pincer-type Au^{III} complexes undergo kinetically controlled self-assembly, which can be devised to follow the living supramolecular polymerization, is described. A qualitative kinetic model[43] was applied to explain the pathway complexity of the supramolecular self-assembly of pincer Au^{III} complexes. Excited states with mixed $^{1/3}$LMMCT and $^{1/3}[\pi-\pi^{*}]$ character have been assigned to account for the spectroscopic properties of Au^{III} aggregates based on DFT/TDDFT calculations and experimental observations.

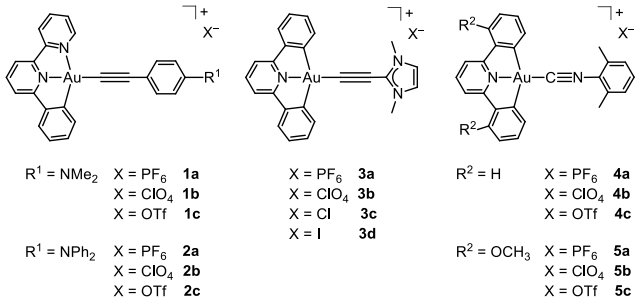

Scheme 1. Chemical Structures of Au^{III} Complexes.

Results

Complexes **1a-b**, **2a-c** were synthesized by the reactions between $[Au(C^N^N)OAc]^+$ and the corresponding acetylene according to the reported procedures with modifications;[8,9] among these compounds, complex **1a** has been reported with its X-ray crystal structure. In the crystal structure, complex **1a** was observed to be packed in a head-to-tail style, and the Au-Au distance is characterized to be approximately 3.49 Å. Complexes **3a-d** were synthesized according to the literature[17] procedure for preparing a series of pincer-type Au^{III} complexes with different allenylidene ligands. Complexes **4a-c**, **5a-c** were synthesized by treatment of [Au(C^N^C)Cl] with 2,6-dimethylphenyl isocyanide and an excess of salt (NH_4PF_6 or KPF_6, $LiClO_4$, AgOTf or LiOTf) in dry CH_3CN solution under Ar for 12 h. Complexes **4a-c** are relatively stable in the solid state (gradually decomposed after approximately 1 week under air; **4c** is the most unstable one), but they are highly sensitive to water in the solution state and quickly decomposed when water is added to their acetonitrile solution (within ten minutes). Compared to **4a-c**, complexes **5a-c** with electron-donating OCH_3 substituents on the [C^N^C] ligand scaffold show better stability in both solution and the solid state. In a water and acetonitrile solution mixture, both **5a** and **5c** are stable for several hours; complex **5b** is stable in solution state with no decomposition within one week. For the unreported stable Au^{III} complexes (**1b-2c**, **3a-d**) studied in this work, NMR spectroscopy, high-resolution mass spectrometry and element analysis were used for characterization. For relatively unstable complexes **4a-5c**, NMR spectroscopy and high-resolution mass spectrometry were combined to characterize these complexes. Furthermore, the X-ray crystal structure of complex **3d** was determined.

Supramolecular Polymerization of Complexes 1 and 2

Complexes **1a-c**, **2a-c** in CH_3CN (1×10^{-4} M) display moderate absorption bands at approximately 400-600 nm (Figure S1). When a mixed solvent of H_2O/CH_3CN was used, a broad redshifted absorption band appeared, indicating the formation of aggregate species. A kinetically controlled supramolecular polymerization process was revealed for **1a** and **1b** in the mixed solvent of H_2O and CH_3CN (9:1 v/v). In Figure 1a-d, a new broad band at approximately 530 nm gradually appeared for **1a** and **1b** in the time course of the experiment. Decreasing the complex concentration slowed down this process. The lag time shown in Figure 1d (1.5×10^{-4} M) for **1b** indicates the existence of a metastable aggregate state that prohibited spontaneous aggregation. By changing the counteranion from ClO_4^- (**1b**) to PF_6^- (**1a**), the lag time, indicating the presence of a kinetically metastable state, disappeared (black line in Figure 1b at a concentration of 1×10^{-4} M). We propose that the energy barrier between the metastable and thermodynamic aggregates is much higher for **1b** than for **1a**. As a result, the high kinetic barrier of **1b** seriously retarded the transformation between these two aggregate states.

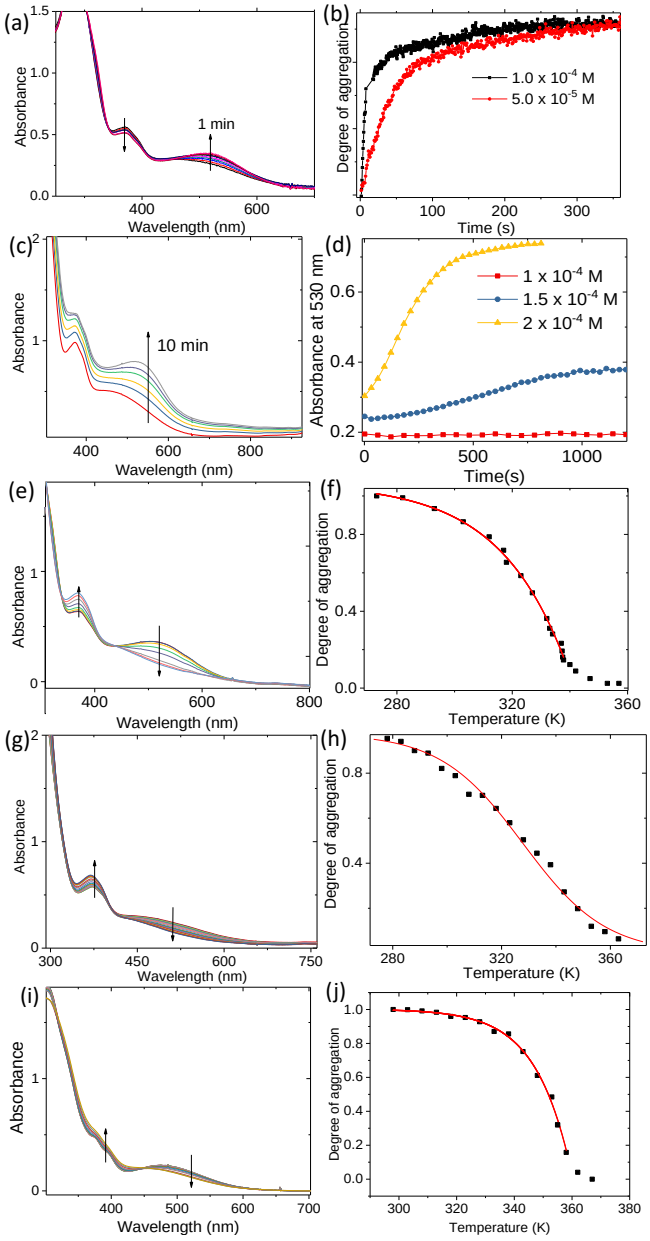

Figure 1. (a) Time-dependent UV/Vis absorption spectral changes of **1a** (1×10^{-4} M, H_2O/CH_3CN, 9:1, v/v) at 298 K. (b) Time-dependent degree of aggregation of **1a** calculated from the absorbance at 530 nm at the indicated concentration. (c) Time-dependent UV/Vis absorption spectral changes of **1b** (2×10^{-4} M, H_2O/CH_3CN, 9:1, v/v). (d) Time-dependent absorbance change of **1b** at 530 nm at the indicated concentration. (e, g, i) Temperature-dependent UV/Vis absorption spectral changes of (e) **1a**, (g) **1c** and (i) **2a** upon heating at a concentration of 1×10^{-4} M (H_2O/CH_3CN, 9:1, v/v). (f, h, j) Plot of the degree of aggregation (black dot) as a function of temperature and the fitting curve (red line) of (f) **1a**, (h) **1c** and (j) **2a**.

Under the same conditions, no time-dependent UV/Vis absorption changes appeared for complexes **1c** and **2a-c**. Upon increasing the temperature, changes in the absorbance for **1a** at 530 nm (thermodynamic aggregate) are indicative of a cooperative mechanism (Figure 1e-f) for the self-assembly process. By fitting the absorption spectral changes with a cooperative model,[29] an elongation temperature of T_e = 341 K and an enthalpy release of ΔH = -9.9 kcal/mol were obtained. For **1c**, the changes in the UV/Vis absorbance at 500 nm upon changing the temperature could be explained by the isodesmic supramolecular polymerization mechanism. A melting temperature of T_m = 328 K and an enthalpy release of ΔH = -15.4 kcal/mol were obtained by fitting the absorption changes (Figure 1g-h) with the isodesmic model. Upon changing the substituent group from NMe_2 (**1a**) to NPh_2 (**2a**) in the acetylene ligand, a greater entropy release of ΔH = -20.9 kcal/mol was obtained, by fitting the temperature-dependent degree of aggregation to the cooperative self-assembly model (Figure 1i-j). The relatively large non-covalent bond formation energy indicates less dynamic features of **2a** (compared with that of **1a**) and therefore, disfavoring **2a** undergoing kinetically controlled self-assembly process.

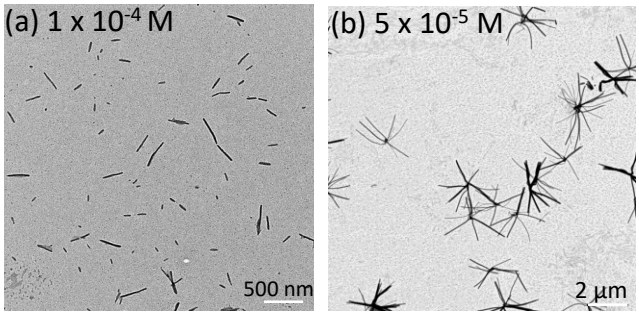

Figure 2. TEM images of **1a** at (a) 1 × 10^{-4} M and (b) 5 × 10^{-5} M in H_2O/CH_3CN (9:1 v/v).

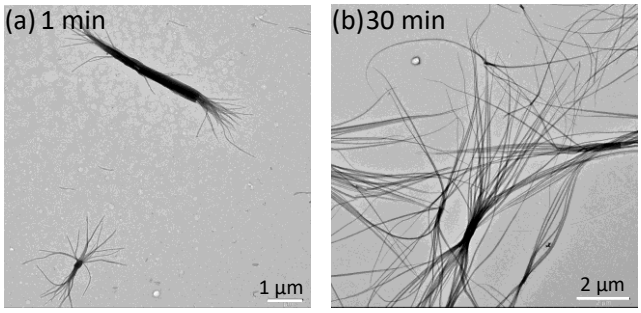

Figure 3. Time-dependent TEM changes of **1b** at (a) 1 min and (b) 30 min (1 × 10^{-4} M, H_2O/CH_3CN, 9:1 v/v).

As the concentration of a complex can make a significant difference in the kinetics of its supramolecular polymerization, we assessed the nano-morphologies of **1a** by TEM images at different concentrations (Figures 2 and 3). When the self-assembly process of **1a** was conducted at a relatively high concentration (1 × 10^{-4} M, Figure 2a), short 1D nanowire structures were observed. In contrast, when the experiment was performed at a relatively low concentration (5 × 10^{-5} M, Figure 2b), two-dimensional (2D) nano-star-shaped structures were observed. The structures featured a nucleus with diameters of approximately 100-200 nm and elongated polymers with a length of approximately 2 µm. The morphologies of the supramolecular polymers were found to be highly dependent on the counteranion. We monitored the time-dependent morphology change in **1b** at a concentration of 1 × 10^{-4} M (Figure 3). In the TEM images, short nanowires emerged in the initial stage. Gradually, thin and long nanowires began to grow at the terminals of the nucleus, leading to 2D bowknot-shaped structures.

Living Supramolecular Polymerization of Complex 1

The supramolecular polymerization of **1b** at a low concentration (below 1 × 10^{-4} M) was monitored by UV/Vis absorption spectroscopy, and the transformation from kinetic aggregates to thermodynamic aggregates was found to be very slow (red line in Figure 1d at a concentration of 1 × 10^{-4} M). The long lag time is tentatively attributed to the high energy barrier between the thermodynamic self-assemblies and kinetic self-assemblies; however, such a barrier can be bypassed by adding a seed. Therefore, we prepared a seed from **1a** (2 × 10^{-5} M) to facilitate the direct aggregation of **1b** (5 × 10^{-5} M) into a final stable aggregate state during the supramolecular polymerization process.

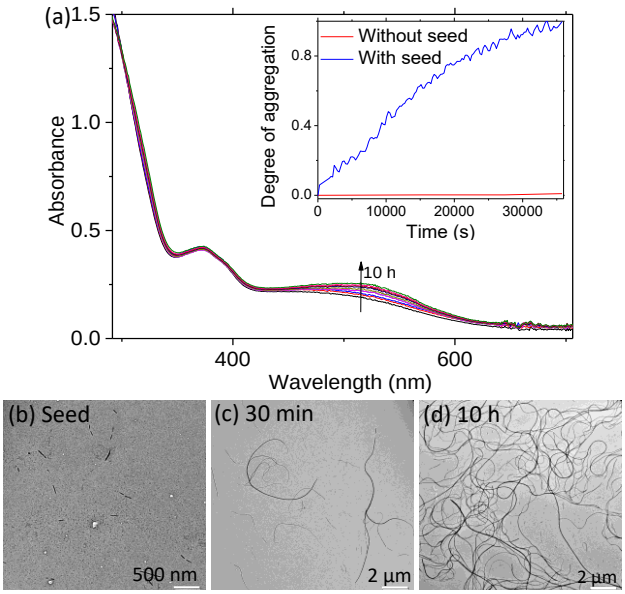

Figure 4. (a) Time-dependent UV/Vis absorption spectra of **1b** with the aid of a seed prepared from **1a** (**1b**, 5 × 10^{-5} M; seed **1a**, 2 × 10^{-5} M). Inset: degree of aggregation calculated at 530 nm for **1b** with and without the seed in the time course of the experiment. (b) TEM image of the seed. (c) and (d) Time-dependent TEM images of **1b** with the seed obtained at 30 min and 10 h, respectively.

As depicted in Figure 4a, after adding the seed to an acetonitrile solution of **1b** at 5 × 10^{-5} M, the lag time disappeared, indicating an externally seeded self-assembly growth process. The length of the seed was approximately 200 nm, as shown in Figure 4b. The time-dependent evolution of the aggregation process was recorded by following the TEM images, as depicted in Figure 4c-d. According to our previous work on counteranion-modulated supramolecular polymerization processes and computational studies,[16,22,44] the PF_6^- counteranion displays weaker intermolecular interactions than the ClO_4^- counteranion with cationic complexes. In

this work, upon breaking the Au^{III} complex cation-PF_6^- interaction, aggregates with different packing forms are proposed to be formed, which was mainly driven by the "cation-cation" dispersive interaction. For the seeded supramolecular polymerization process of **1b**, the use of **1a** (PF_6^- counteranion) as a seed helped break the Au^{III} complex cation-ClO_4^- interaction, thereby facilitating the growth of its thermodynamic aggregates. To further prove the external seeded supramolecular polymerization, we performed two control experiments, monitoring the self-assembly of complex **1b** without seed **1a** and seed **1a** in the absence of **1b** by UV/Vis absorption spectroscopy (Figure S3).

Supramolecular Polymerization of Complex 3 and X-ray Crystal Structure

Organometallic complexes containing N-heterocyclic allenylidene (C=C=CRR$^{\cdot}$) ligands are usually stable and exhibit intriguing photoluminescence, metallophilic interactions and cytotoxicity properties.[45] Complexes **3a-d** were prepared with N-heterocyclic allenylidene ligands, and these complexes are stable in both the solid state and solution. The crystal structure of **3d** shows a zig-zag Au-Au chain structure, featuring a close Au-Au contact of approximately 3.367 Å, with complex cations arranged in a skewed fashion, as shown in Figure 5.

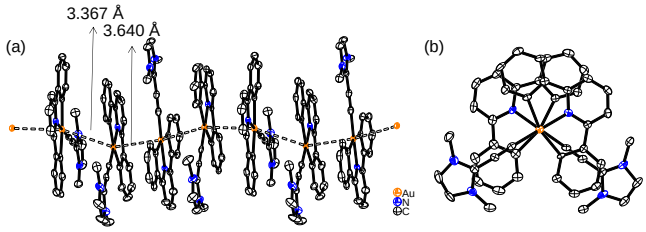

Figure 5. (a) X-ray crystal structure of **3d** featuring a zig-zag structure with close alternating Au-Au contacts of 3.367 Å and 3.640 Å. Hydrogen atoms and counteranions are omitted for clarity. (b) Top view of the dimeric Au^{III}-Au^{III} structure.

Complexes **3a-d** in CH_3CN (1×10^{-4} M), which are presumably in a discrete monomeric form, display two moderate absorption bands at approximately 380 and 400 nm (Figure S5-S6). When a mixed solvent of H_2O/CH_3CN was used, two redshifted absorption bands at approximately 400 nm and 420 nm appeared for **3a**, indicating the formation of aggregate species (Figure 6a). Time-dependent UV/Vis absorption spectral changes and stepwise self-assembly process were observed for this complex. As shown in Figure 6a, upon injecting water into an CH_3CN solution of **3a**, two new absorption bands at approximately 400 and 420 nm gradually emerged; this behavior is indicative of the presence of a kinetically trapped aggregate state during the self-assembly pathway. Lowering the concentration of **3a** slowed down this process. As shown in Figure 6b, lag times of ~100 s and ~300 s were observed when the measurements were conducted at concentrations of 5×10^{-5} M and 3×10^{-5} M, respectively. For aggregates **3b-d** in the mixed solvent of H_2O/CH_3CN, absorption bands at around 392 nm and 412 nm appeared instantly with no time-dependent changes in Figure S5-S6. The absorption spectra of aggregates **3b-d** are similar to that observed for **3a**-kinetic aggregate in Figure 6a.

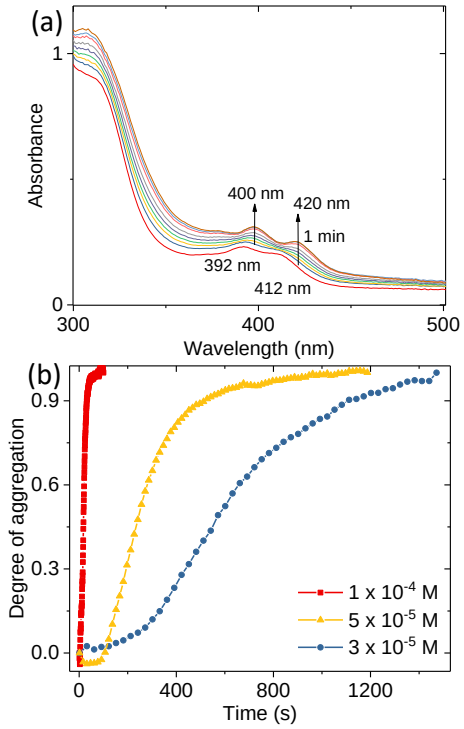

Figure 6. (a) Time-dependent UV/Vis absorption spectral changes of **3a** (1×10^{-4} M, H_2O/CH_3CN = 9:1, v/v) at 298 K. Inset: amplification of the change in the absorbance at 400 and 420 nm in the time course of the experiment. (b) Degree of aggregation of **3a** calculated from the absorbance at 420 nm at the indicated concentration in the time course of the experiment.

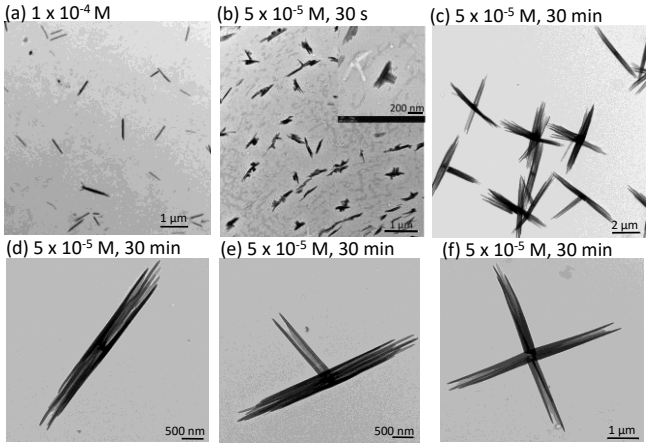

Figure 7. TEM images of **3a** at (a) 1×10^{-4} M in H_2O/CH_3CN (9:1 v/v). TEM images of **3a** at 5×10^{-5} M in H_2O/CH_3CN (9:1 v/v) obtained at (b) 30 s and (c-f) 30 min.

The morphology of the nanostructures is highly dependent on the concentration of **3a** in the mixed CH_3CN/H_2O solution (Figure 7). When the self-assembly process was conducted at a concentration of 1×10^{-4} M, a 1D nanowire morphology (with a length of approximately 1 μm) was observed. However, upon lowering the concentration to 5×10^{-5} M, polymers characterized by a nucleus and elongated wires emerged in a stepwise manner. Changes in time-dependent

TEM images were monitored and captured: initially, a small nucleus with a length of ~200 nm appeared (Figure 7b), followed by the Au^{III} complexes growing at the terminals of the nucleus, leading to 2D supramolecular polymers (with a size of approximately 3-4 μm), as shown in Figure 7d-f. By replacing the PF_6 counteranion with other counteranions, small nanoparticle structures (with a diameter of approximately 50 nm) were observed for **3b-d** and showed no obvious relationship with the complex concentration upon aggregation (Figures S7-S8). In its aggregate form, complex **3d** showed weak phosphorescence with an emission maximum at ~500 nm, as shown in Figure S9.

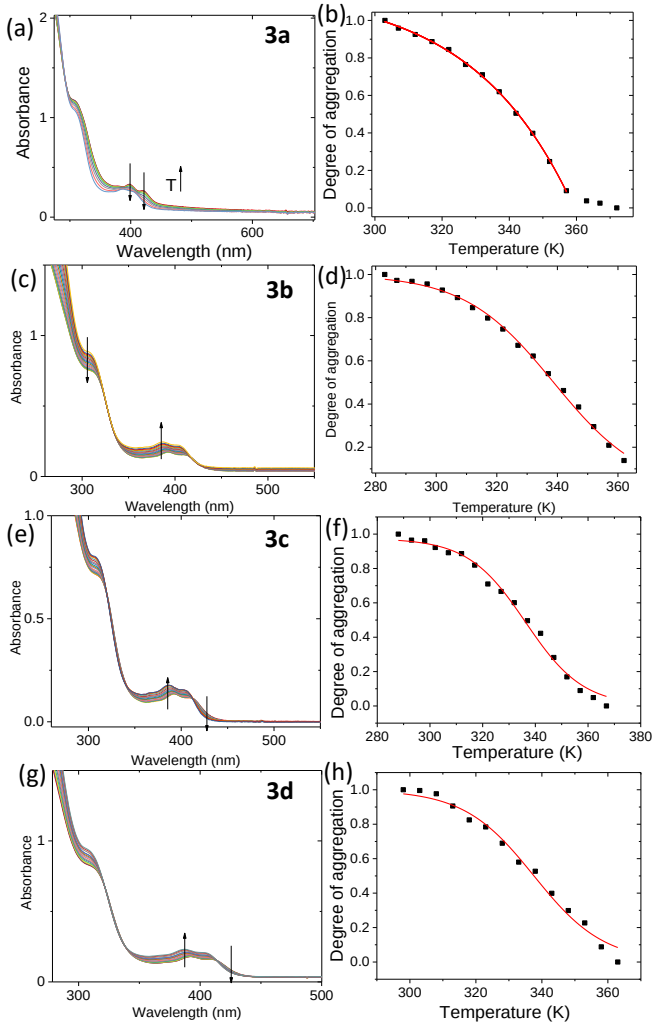

Figure 8. Temperature-dependent UV/Vis absorption spectral changes of (a) **3a**, (c) **3b**, (e) **3c** and (g) **3d** at the concentration of 1×10^{-4} M in H_2O/CH_3CN (9/1, v/v) upon heating. Plot of the degree of aggregation (black dot) as a function of temperature and the fitting curve (red line) of (b) **3a**, (d) **3b**, (f) **3c** and (h) **3d**.

We performed temperature-dependent UV/Vis measurements for **3a-d** in the mixed H_2O/CH_3CN solvent, to probe the difference of their supramolecular polymerization mechanism by changing counteranions. As shown in Figures 8a-b, the changes in the degree of aggregation for **3a** could be fitted with the cooperative nucleation-elongation model, from which an elongation temperature of T_e = 359 K and an enthalpy release of ΔH = -8.5 kcal/mol were obtained. In contrast, complex **3b-d** followed sigmoidal isodesmic self-assembly model as shown in Figures 8c-h. The non-covalent bond formation entropy and melting temperature were determined to be -17.2 kcal/mol and 335 K for **3b**, -21.8 kcal/mol and 335 K for **3c**, -22.5 kcal/mol and 338 K for **3d**, respectively. The relatively large non-covalent bond formation energy for **3b-d** (compared with that of **3a**) during the aggregation process suggests their less dynamic features, which is considered to be one of the reasons that leads to the absence of a kinetically controlled self-assembly process for **3b-d**.

Phosphorescent Au^{III} Aggregates of Complexes 4 and 5

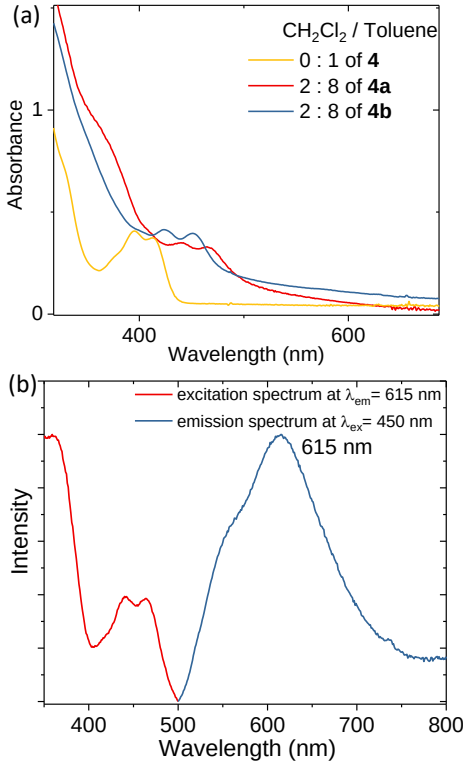

Figure 9. (a) Solvent-dependent UV/Vis absorption spectra of **4a** and **4b** (1×10^{-4} M) at 298 K. The absorption spectra on **4a**, **4b** and **4c** in a monomeric state in CH_2Cl_2 showed no differences. (b) Emission and excitation spectra of **4a** (1×10^{-4} M, CH_2Cl_2/toluene = 2/8, v/v) at 298 K.

Au^{III} complexes **4a-c** with isocyanide auxiliary ligands are sensitive to water and were observed to decompose after long-term standing under air in the solution state (Figures S10-S11). Therefore, we used dry toluene to induce supramolecular polymerization in CH_2Cl_2 solution. The UV/Vis absorption spectrum of **4** in CH_2Cl_2 (presumably in a discrete monomeric state) is shown in Figure 9a, together with the spectrum recorded in mixed CH_2Cl_2/toluene (2:8, v/v) corresponding to the aggregate state. Complex **4** in CH_2Cl_2 solution (1×10^{-4} M) shows moderate absorption bands at 395 and 415 nm. Upon aggregation, two new absorption bands of the aggregate species appeared at 420 and 445 nm for **4b** and at 443 and 470 nm for **4a**. Complex **4a** was found to be emissive in the aggregate state (1×10^{-4} M, CH_2Cl_2/toluene, 2:8, v/v), featuring a broad emission peak at 615 nm, as shown in Figure 9b. For **4c**, a new absorption band at approximately

450 nm gradually appeared, and the polymerization rate was found to be related to the complex concentration, as shown in Figure S13.

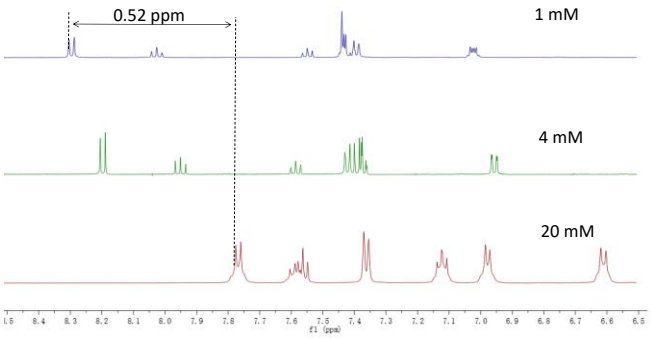

Figure 10. Concentration-dependent ^{1}H NMR spectra for **5a** in CD_3CN at 298 K.

Compared to **4a-c**, Au^{III} complexes **5a-c** show better stability in both the solid and solution state. In concentration- (Figure 10) and temperature-dependent ^{1}H NMR spectra (Figure S17) of **5a**, an upfield change in the chemical shifts was observed upon increasing the concentration or lowering the temperature. The formation of π - π stacked aggregate species accounted for the change in chemical shifts, which were influenced by the ring current of the aromatic groups.[46,47] In Figure 10, it can be noted that upon increasing the concentration from 1 mM to 20 mM, complex **5a** showed an upfield chemical shift change of 0.52 ppm.

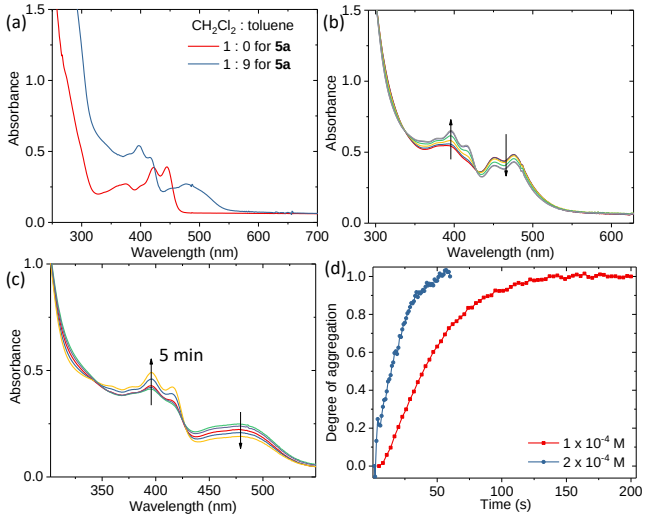

Figure 11. (a) Solvent-dependent UV/Vis absorption spectral changes for **5a** (1 × 10^{-4} M) at 298 K. (b) Time-dependent UV/Vis absorption spectral changes for **5b** at 298 K (1 × 10^{-4} M, CH_2Cl_2/toluene = 1/9, v/v). (c) Time-dependent UV/Vis absorption spectral changes for **5c** in CH_2Cl_2/toluene (1/9, v/v) at 1 × 10^{-4} M. (d) Time-dependent degree of aggregation for **5b** calculated from the absorbance at 480 nm at the indicated concentration in CH_2Cl_2/toluene (1/9, v/v).

UV/Vis absorption spectra for **5a** in the monomeric state (in CH_2Cl_2) and aggregate state (in CH_2Cl_2/toluene, 1:9, v/v) are displayed in Figure 11. Complex **5a** in CH_2Cl_2 solution (1 × 10^{-4} M) shows two moderate absorption bands at 420 and 445 nm. Upon aggregation, a new broad absorption band at 485 nm emerged for **5a** and **5c**, while two new absorption bands at 450 and 480 nm appeared for **5b** (Figure 11b). Kinetically controlled supramolecular polymerization process were observed for **5b-c**, reflected by the time-dependent absorption spectral changes and the influnce of concentration on the rate of the self-assembly process (Figure 11b-d). The kinetically controlled self-assembly of complex **5b** showed acceleration upon increasing the complex concentration (Figure 11d).

Complexes **5a-c** were found to be nearly non-emissive in the monomeric state, while they display moderate emission intensity in the aggregate state (1 × 10^{-4} M, CH_2Cl_2/toluene, 1:9, v/v). The aggregates of **5a-c** exhibit a broad emission peak at 560, 605, and 565 nm, respectively, as shown in Figure 12. High phosphorescence quantum yields up to 61% have been reported for charge neutral pincer-type Au^{III} complex in solutions.[49,50] However, for cationic Au^{III} complexes, only moderate emission quantum yield of ~13% could be achieved, such as that in $[Au^{III}(C\text{^}N\text{^}C)L]^+$ (L=N-heterocyclic carbene) system.[51] As the coordinated NHC ligand is orthogonal to the [Au(C^N^C)] plane, intermolecular interaction and aggregation is disfavored. Thus the $[Au^{III}(C\text{^}N\text{^}C)L]^+$ system was not chosen for this work. According to the measured emission quantum yield (1%-6%) and excited lifetime (0.5-4 μs) for **5a-c**, the k_r (radiative decay rate) values were calculated to be 1.5-2.1 × 10^4 s^{-1}, which are higher than those of reported Au(C^N^C)-alkyl complexes (intraligand excited state in nature with k_r of approximately 2 × 10^3 s^{-1}).[48] The increased k_r values indicate the involvement of Au-metal characters in the frontier molecular orbitals of the excited state (LMMCT transition revealed by the DFT/TDDFT calculations discussed later), facilitating the ISC (inter-system crossing process) and the $T_1 \rightarrow S_0$ transition.

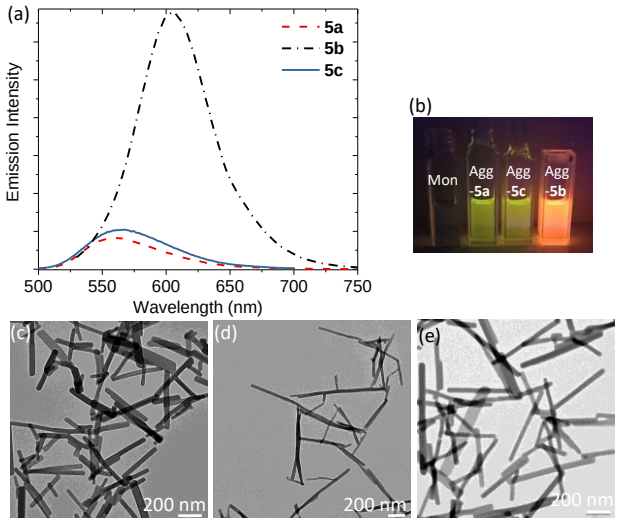

Figure 12. (a) Emission spectra of **5a-c** in the aggregate state (1 × 10^{-4} M, CH_2Cl_2/toluene = 1:9, v/v) at 298 K. Complexes **5a-c** in the monomeric state in CH_2Cl_2 showed no observable emission. (b) From left to right: emission color of monomer-5 in CH_2Cl_2 and aggregate-**5a**, aggregate-**5c**, and aggregate-**5b** in the mixed solvent (CH_2Cl_2/toluene = 1:9, v/v) at 1 × 10^{-4} M (λ_{ex} = 365 nm). TEM images of (d) **5a**, (e) **5b** and (f) **5c** at 1 × 10^{-4} M in the mixed solvent of CH_2Cl_2 and toluene (1:9, v/v).

DFT/TDDFT Calculations and Excited States of Phosphorescent Au^{III} Aggregates

DFT/TDDFT calculations were directly performed on the X-ray crystal structures of **1a** and **3d** without further optimization. As there is no available X-ray crystal structure for **4**, we first optimized the structures of $[\mathbf{4}]_2$ and $[\mathbf{4}]_4$ in the head-to-tail arrangement and then performed the subsequent calculations on the optimized structures. As revealed by the calculated absorption spectrum (Figure 13a) for **3**, the lowest absorption band for the dimer showed a slight redshift (from 371 nm for the monomer to 395 nm for the dimer). From experimental observations, the lowest absorption band of complex **3** redshifted from 400 to 420 nm upon aggregation. In the TDDFT calculations, the lowest energy absorption bands for the monomer and dimer are mainly from the HOMO→LUMO transitions. Further investigations by the molecular orbital (MO) diagrams (Figure 13b) of monomer **3** show the involvement of minor $Au^{III}(6p_z)$ orbitals in the LUMO together with the major component of the π orbital from the ligand. In dimer $[\mathbf{3}]_2$, a weak bonding orbital σ ($6p_z$) is proposed to be formed between two Au^{III} centers and to become the new LUMO with lower energy. Therefore, the nature of the excited state of **3** upon aggregation is assigned to mixed minor ^{1}LMMCT and major ^{1}[π - π*] transitions. A similar case was found for complex **4** upon aggregation: The excited states for $[\mathbf{4}]_2$ and $[\mathbf{4}]_4$ originate from the mixed ^{1}LMMCT and ^{1}[π - π*] transitions (Figure S22). By contrast, for **1**, the excited state of the aggregated species is assigned to the ^{1}[LLCT] (ligand-to-ligand charge transfer) transition localized on the ligands with no Au^{III} contribution (Figure S21).

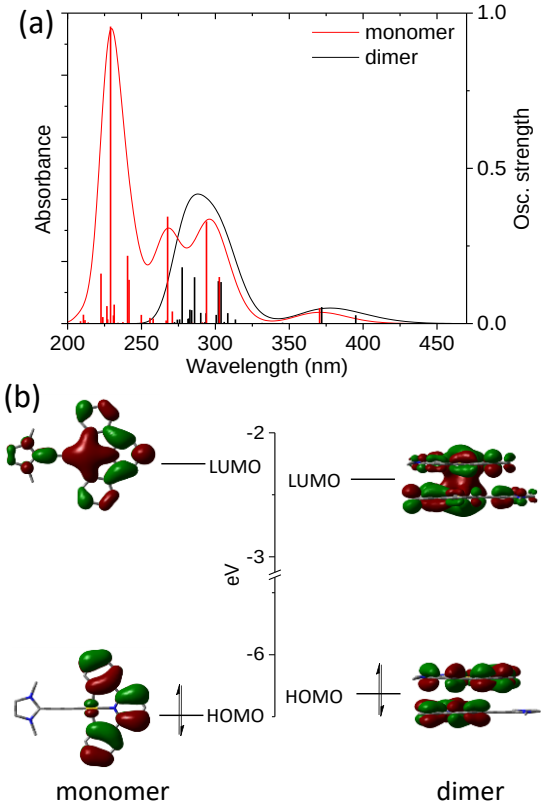

Figure 13. Calculated (a) absorption spectra and (b) MO diagram of **3** and dimer $[\mathbf{3}]_2$ in the S_0 state.

By adding electron-donating OMe groups to the pincer-type ligand of **4** to give **5**, the energy of π* orbital (located at ligand C^N^C) is destabilized, rendering more component of Au^{III} $6p_z^2$ orbital in the LUMO. Therefore, we observed the formation of a broad redshifted absorption/emission band (instead of a vibronic band) and increased k_r constants at aggregate states for **5a**, which indicates the formation of an excited state with charge transfer properties and the involvement of more Au^{III} $6p_z^2$ orbital component in the LUMO.

Discussion

Au^{III}-Au^{III} Interaction in the S_0 and T_1 States and the Nature of the $^{1/3}$LMMCT Transition

To address the question as to whether an attractive Au^{III}-Au^{III} bonding interaction exists or not in pincer-type Au^{III} complexes, we also studied their isoelectronic counterparts, the pincer Pt^{II} and Pd^{II} complexes, which are well documented to display M-M interactions (in both the S_0 and T_1 states), for reference and comparison.

In some early semiempirical models,[52] the attractive closed-shell d^8-d^8 interaction was considered to arise mainly from the orbital term[53] and was induced by the relativistic effects of heavy atoms, as reflected by the large radial contraction of s/p orbitals and radial expansion of d/f orbitals.[54] However, recent theoretical studies stated that M-M orbital interactions are less important than intermolecular dispersion interactions.[8,53,55,56] In this work, relativistic and dispersion effects on the Au^{III}-Au^{III} interaction in the S_0 ground state were considered and evaluated. By taking into account the relativistic effect of the heavy Au^{III} atom, the $6p_z$ orbital is stabilized and becomes lower in energy, compared to the one without considering the relativistic effect (Figure S19). Similar to recently reported computational studies, the calculation results indicate that the ligand-ligand dispersive interaction is the major driving force for the self-assembly process of Au^{III} aggregates (Figure S20). Although closed-shell M-M orbital interaction is not always the driving force for the dimerization/oligomerization process of organometallic complexes, the interactions among different orbitals between two monomers will generate new electronic configurations in the dimer structure. Therefore, a distinct excited state with lower energy will appear for the dimer/oligomer species, which is one of the most important findings obtained by studying M-M orbital interactions. In the following section, to determine the electronic configurations and excited states in the dimer/aggregate forms of Au^{III} complexes, main attention is paid to M-M orbital interactions (instead of M-M dispersion interactions or other noncovalent interactions).

For the d^8-d^8 metal complexes where the metal is Pd^{II} or Pt^{II}, the overlap of two d_z^2 orbitals in the axial direction between two metal cations results in the destabilization of the orbital $\sigma^*(d_z^2)$. Therefore, the antibonding $\sigma^*(d_z^2)$ between two metal cations becomes the new HOMO of the dimer/oligomer species.[57] A qualitative molecular orbital model for d^8-d^8 metal complexes in the ground state is given in Figure S23.

However, the energy of the $5d_z^2(Au^{III})$ orbital would be relatively lower for the Au^{III} complexes studied in this work than for the Pt^{II}/Pd^{II} complexes, as the Au^{III} cation is more electrophilic in nature. The HOMO of the pincer-type Au^{III} complexes would mainly localize on the tridentate ligand. Weak d orbital overlap, if any, is expected in this series of Au^{III} complexes. Moreover, the $6p_z$ orbital of Au^{III} would be

much lower lying in energy than the $6p_z(Pt^{II})$ and $5p_z(Pd^{II})$ orbital and is considered to make some contributions to the LUMO.

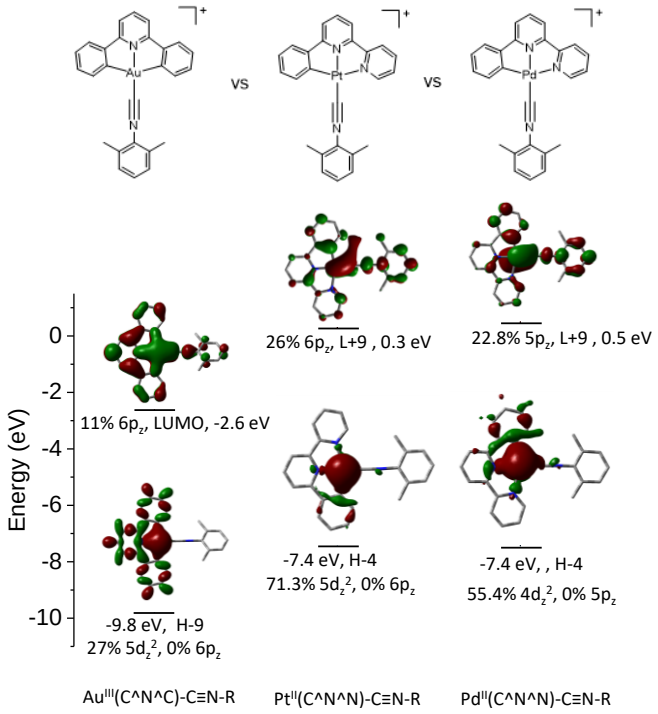

Figure 14. MO diagrams of **4** and its isoelectronic Pt^{II} and Pd^{II} counterparts [(C^N^N)MC≡N(2,6-dimethylphenyl)] (M = Pt or Pd) in the optimized S_0 structures.

We performed DFT calculations to compare Au^{III} complex **4** with its isoelectronic Pt^{II}/Pd^{II} counterparts [(C^N^N)MC≡N(2,6-dimethylphenyl)] (M = Pt or Pd) in the ground state (Figure 14). The energies and proportions for nd_z^2 and $(n+1)p_z$ orbitals are displayed for all Au^{III} and Pt^{II}/Pd^{II} complexes. From Figure 14, the energy of the nd_z^2 orbital in the Au^{III} complex is much lower than that of the Pt^{II}/Pd^{II} complexes (differs by approximately 2.4 eV), which is consistent with the electrophilic nature of the Au^{III} cation. For the $(n+1)p_z$ orbital, the one in the Au^{III} complex is approximately 2.9 eV lower than that in its Pt^{II}/Pd^{II} counterparts, causing the $6p_z$ orbital to become part of the LUMO in the Au^{III} complex.

In the Au^{III} dimer's MO diagram (Figure 15), small splitting between the two Au(5d σ *) and Au(5d σ) orbitals (~0.5 eV) emerged with a minor contribution from the Au($6p_z$) orbital of approximately 0.5%, indicating a weak Au-Au orbital interaction in the ground state (compared to the Pt-Pt/Pd-Pd orbital interactions shown in Figure S25). At the same time, the bonding 6p σ orbital became the new LUMO in the Au^{III} dimer, and therefore, a new excited state will be generated upon excitation. A qualitative electronic configuration of the Pt^{II}-Pt^{II}/Pd^{II}-Pd^{II} and Au^{III}-Au^{III} dimers in excited state T_1 is displayed in Figure S24. In the case of the Au^{III} dimer, upon excitation, an electron in the HOMO or a lower energy orbital (ligand π) would be excited to the LUMO, which can be regarded as a weak bonding orbital between two Au^{III} centers. Similar to the Pd^{II}/Pt^{II} dimers, a half bond (or less, depending on the metal character in the LUMO) was proposed to be formed in this Au^{III}-Au^{III} system in the T_1 excited state.

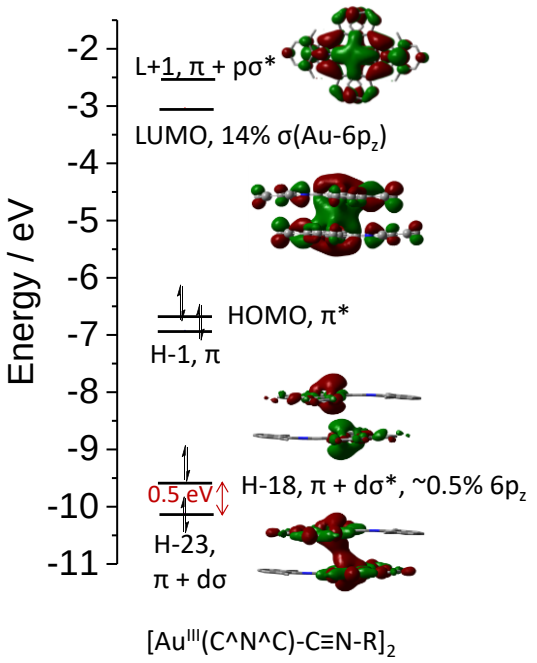

Figure 15. MO diagram of Au^{III} dimer $[\mathbf{4}]_2$ in the optimized S_0 structure.

The attractive Au^{III}-Au^{III} bonding interaction in the T_1 excited state was further elucidated by the DFT/TDDFT calculation results. The optimized triplet excited state geometry of $[\mathbf{4}]_2$ reveals a shortening of the Au-Au distance from 3.56 Å in S_0 to 3.39 Å in the T_1 state (Figure 16). This finding is supportive of the existence of attractive Au^{III}-Au^{III} interactions in the T_1 state.

The nature of the emissive excited state for the Au^{III} dimer in T_1 was assigned to the mixture of major ^{3}[π - π *] and minor ^{3}LMMCT transitions shown in Figure 16b. From the MO diagrams, it can be noticed that the 6p σ orbital delocalized onto the two Au^{III} centers in the LUMO. The emission energy of $[\mathbf{4}]_2$ in the T_1 state was calculated to be 2.3 eV, which is close to the experimental value of 2.0 eV (Figure 9).

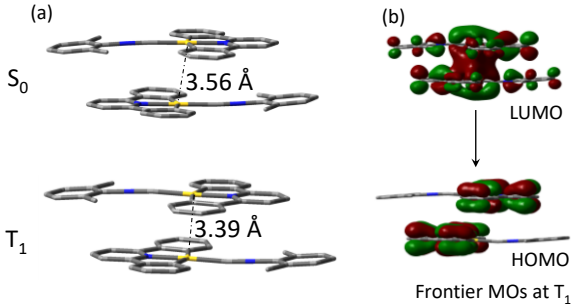

Figure 16. (a) Optimized dimer structures of $[\mathbf{4}]_2$ in the S_0 (top) and T_1 (bottom) states. (b) FMO diagram of $[\mathbf{4}]_2$ in the optimized T_1 structure.

Although a bonding metal-metal interaction was considered formed in both of the Pt^{II}-Pt^{II}/Pd^{II}-Pd^{II} and Au^{III}-Au^{III} cases in the T_1 state, the nature of the ^{3}MMLCT and ^{3}LMMCT excited states is distinctly different. In the Pd^{II}/Pt^{II} case, upon excitation, the Pd^{II}/Pt^{II} cation would be oxidized, while the π -conjugated ligand would be reduced as the

charge transfers from the metal to the ligand (MMLCT). By contrast, for the Au^{III}-Au^{III} dimer in the excited state, the metal cation would be reduced by the ligand during the reverse charge transfer flow of the LMMCT. The change in the charge transfer flow was considered to have significant influence on the photophysical, photochemical and semiconducting properties of the d^8 organometallic complexes. We conceive that Au^{III} complexes possess promising potential in the design of supramolecular materials with new functions as a result of their unique electronic properties and distinct excited states.

Pathway Complexity of Complexes 1 and 3

To account for the counteranion- and/or concentration-dependent kinetics and supramolecular polymer morphologies observed for **1** and **3**, a qualitative kinetic model is applied.[28,43] As shown in Figure 17, symbol A represents the monomer, A_n is the aggregate species having n monomers, and n represents the size of the nucleus.

A four-step self-assembly mechanism was used to account for the systems studied here: (Step 1) At first, Au^{III}-counteranion complex is soluble in CH_3CN/CH_2Cl_2 and would be surrounded by solvent molecules in these solvents. The counteranion has relatively close contact with complex cation in the organic solvent cage at this stage. (Step 2) Upon injecting a poor solvent (water or toluene) into a solution (CH_3CN or CH_2Cl_2) of the complex, the solvent cage is disrupted and the monomers would be quickly trapped in the kinetic aggregate state A_n^*, termed the "inactive nucleus". As there is no decent energy barrier between monomer A and inactive nucleus A_n^*, this process occurs very quickly and spontaneously. The counteranion still has relatively close contact with Au^{III} complex at this kinetic aggregate state. (Step 3) By breaking the electrostatic interaction between the counteranion and complex cation, the inactive nucleus is slowly transformed into "active nucleus" A_n. This process is counteranion dependent, and the activation energy barrier is significantly affected by the interaction between the complex cation and counteranion. This transformation process is also considered to be the rate-determining step which is responsible for the induction period (lag time) observed for **1b** and **3a** (Figure 1d & 6b). (Step 4) If there are excess remaining monomers in the solution, these monomers will further aggregate at the terminals of the activated nucleus, which is termed the elongation process as shown in Figure 17.

In summary, there are three types of molecules and four types of intermolecular interactions involved during the kinetically controlled self-assembly process: cationic Au^{III} complex, counteranion and solvent molecule (mixed solvent); cation-cation interaction, cation-counteranion interaction, counteranion-counteranion interaction and solvation energy (which could be further decomposed to: kinetic aggregate's solvation energy, thermodynamic aggregate's solvation energy and monomer's solvation energy). The transformation from kinetic aggregate to thermodynamic aggregate is accelerated by the following non-covalent interactions: strong cation-cation dispersive interaction; weak cation-anion interaction; less kinetic-aggregate's solvation energy and more thermodynamic-aggregate's solvation energy. Change of the metal complex (ligand or metal) influences the cation-cation interactions (Ligand-Ligand dispersive, Metal-Ligand dispersive and M-M closed shell interaction); change of the counteranion influences the cation-counteranion interaction. Change of the solvent (ACN/water or DCM/toluene) affects the solvation energy.

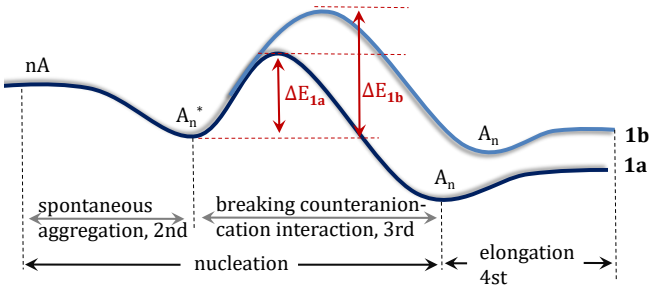

Figure 17. Qualitative energy landscape of the supramolecular polymerization models for **1a** and **1b**.

The following equation, developed by Oosawa and Kasai, was employed to describe the reaction rate of nucleus formation (step 3):[43,58,59]

$$\frac{d[A_n]}{dt} = k^*[A]^n - k_-^*[A_n] - k[A][A_n] + k_-[A_{n+1}] \quad (1)$$

where [A] is the concentration of the monomer; $[A_n]$ is the concentration of the active nucleus; k^* and k_-^* represent the rate constants for the formation and dissociation of A_n (step 3), respectively; and k and k_- are the rate constants of the forward and reverse chain elongation reactions (step 4), respectively.

For the formation rate of the activated nucleus and elongated polymer ($i \geq n$), we have:

$$\frac{dc_p^*}{dt} = \frac{d\sum_{i=n}^{\infty}[A_i]}{dt} = k^*[A]^n - k_-^*[A_n] \quad (2)$$

where c_p^* is the concentration of all polymers equal to or larger than n.

Concentration-Dependent Kinetics for 1a and 3a. According to equations (1) and (2), the formation rates of the active nucleus and elongated polymer are positively correlated with the total monomer concentration [A]. At a high concentration of **1a** and **3a** (1×10^{-4}M), as the nucleation rate is very fast, the monomers will be quickly consumed and transformed into the active nucleus. The depolymerization of the nucleus and elongated polymers can be approximately ignored in this situation. All of the complexes aggregating at the terminal of the nucleus will be instantly activated. Therefore, only short, uniform 1D nanowires emerged (Figure 2a and Figure 7a).

However, upon lowering the concentration of **1a** and **3a**, the rate of the nucleation process (step 3) was slowed down, indicating that excess monomers may remain in the system, together with the transformed active nucleus A_n. The depolymerization of the nucleus cannot be ignored in this situation. Only part of the complexes (at the end of the nucleus) can be activated at a relatively slow rate. Gradually, the remaining monomers in the solution began to elongate along only the activated part of the nucleus (step 4); therefore, 2D supramolecular structures were observed for **1a** and **3a** at relatively low concentrations.

Counteranion-Dependent Kinetics for 1. According to our previous work,[16, 22] PF_6^- (compared with ClO_4^-) would show weaker interactions with the metal complex, leading to a smaller kinetic energy barrier (ΔE_{1a}) for **1a** (counteranion: PF_6^-) than for **1b** (counteranion: ClO_4^-).

According to the Arrhenius equation, the rate constant, k, for a chemical reaction is inversely proportional to the activation energy, $\Delta \boldsymbol{E}$. Therefore, we have:

$$k^*_{1b} < k^*_{1a} \quad (3)$$

According to equation (2), the reaction rate of the polymerization is positively related to the forward rate constant k^*. When $k^*_{1b} < k^*_{1a}$, the nucleation process (step 3) for **1b** will be seriously retarded, which was reflected by the long lag time shown in Figure 1d. During the lag time, a large number of complexes would remain as monomers in the system because of the dissociation of the inactive nucleus. Similarly, only part of the complexes (at the end of the nucleus) can slowly be activated. Upon elongation of the remaining monomers, the 2D bowknot-shaped nanostructure shown in Figure 3b was formed and observed.

CONCLUSIONS

We demonstrated the kinetically controlled self-assembly of phosphorescent pincer-type d^8 Au^{III} aggregates by tuning the counteranion and concentration. Living supramolecular polymerization was achieved for Au^{III} complexes with acetylene as the ligand. A qualitative kinetic model was applied to explain the pathway complexity of Au^{III} complexes studied in this work. A close Au-Au contact of 3.367 Å was observed in the X-ray crystal structure of the Au^{III}-allenylidene complex. A DFT/TDDFT study revealed that pincer Au^{III}-isocyanide and Au^{III}-allenylidene complexes can display weak attractive Au^{III}-Au^{III} interactions upon excitation; furthermore, a mixed $^{1/3}$LMMCT and $^{1/3}\pi$ - π * excited state was assigned to the polymeric Au^{III} species through the supramolecular polymerization.

ASSOCIATED CONTENT

Supporting Information

Experiment procedures, characterization of complexes (including NMR spectra, high resolution mass data and element analysis), computational and experimental details, molecular coordinates by calculations, emission and excitation spectra, UV/Vis absorption spectra, TEM images, and CIF file for the X-ray crystal structure of **3d**.

AUTHOR INFORMATION

Corresponding Author

* cmche@hku.hk

Funding Sources

This work was supported by Hong Kong Research Grants Council (HKU 17303815, 17330416) and Basic Research Program-Shenzhen Fund (JCYJ20160229123546997, JCYJ20170412140251576, and JCYJ20170818141858021)

Notes

The authors declare no competing financial interest.

ACKNOWLEDGMENT

This work was conducted in part using the research computing facilities and/or advisory services offered by Information Technology Services, The University of Hong Kong. We thank Dr. Xin-Shan Xiao and Dr. Xiaoyong Chang for assistance in preparing the allenylidene complexes and solving the X-ray crystal structure of **3d**.

REFERENCES

(1) Schmidbaur, H. Supramolecular chemistry: going for gold. *Nature* **2001**, *413*, 31.

(2) Pyykkö, P.; Mendizabal, F. Theory of the d^{10}-d^{10} closed-shell attraction: 2. long-distance behaviour and nonadditive effects in dimers and trimers of type [(X-Au-L)$_n$] (n = 2, 3; X = Cl, I, H; L = PH_3, PMe_3,-N≡ CH). *Chem. - Eur. J.* **1997**, *3*, 1458.

(3) Pyykkö, P.; Runeberg, N.; Mendizabal, F. Theory of the d^{10}-d^{10} closed-shell attraction: 1. dimers near equilibrium. *Chem. - Eur. J.* **1997**, *3*, 1451.

(4) Schmidbaur, H.; Weidenhiller, G.; Steigelmann, O.; Müller, G. Gold(I) complexes of primary phosphanes: pair formation through Au···Au interactions. *Chem. Ber.* **1990**, *123*, 285.

(5) Cotton, F. A.; Feng, X.; Matusz, M.; Poli, R. Experimental and theoretical studies of the copper(I) and silver(I) dinuclear N,N'-di-p-tolylformamidinato complexes. *J. Am. Chem. Soc.* **1988**, *110*, 7077.

(6) Dietzsch, W.; Franke, A.; Hoyer, E.; Hummel, D, G, H.-U.; Otto, P. New dimeric gold selenolates: preparation and characterization of $[(n\text{-}C_4H_9)_4N]_2[AuSSeC{=}C(CN)_2]_2$ and $[(n\text{-}C_4H_9)_4N]_2[AuSe_2C{=}C(CN)_2]_2$. *Z. Anorg. Allg. Chem.* **1992**, *611*, 81.

(7) Schmidbaur, H.; Graf, D.-C. W.; Müller, G. Weak intramolecular bonding relationships: the conformation-determining attractive interaction between gold(I) centers. *Angew. Chem., Int. Ed.* **1988**, *27*, 417.

(8) Lu, W.; Chan, K. T.; Wu, S.-X.; Chen, Y.; Che, C.-M. Quest for an intermolecular Au(III) ··· Au(III) interaction between cyclometalated gold (III) cations. *Chem. Sci.* **2012**, *3*, 752.

(9) Xiao, X.-S.; Kwong, W.-L.; Guan, X.; Yang, C.; Lu, W.; Che, C.-M. Platinum(II) and gold(III) allenylidene complexes: phosphorescence, self-assembled nanostructures and cytotoxicity. *Chem. - Eur. J.* **2013**, *19*, 9457.

(10) Li, K.; Tong, G. S. M.; Wan, Q.; Cheng, G.; Tong, W.-Y.; Ang, W.-H.; Kwong, W.-L.; Che, C.-M. Highly phosphorescent platinum(II) emitters: photophysics, materials and biological applications. *Chem. Sci.* **2016**, *7*, 1653.

(11) Roundhill, D. M.; Gray, H. B.; Che, C.-M. Pyrophosphito-bridged diplatinum chemistry. *Acc. Chem. Res.* **1989**, *22*, 55.

(12) Wong, K. M.-C.; Yam, V. W.-W. Self-assembly of luminescent alkynylplatinum(II) terpyridyl complexes: modulation of photophysical properties through aggregation behavior. *Acc. Chem. Res.* **2011**, *44*, 424.

(13) Ma, B.; Li, J.; Djurovich, P. I.; Yousufuddin, M.; Bau, R.; Thompson, M. E. Synthetic control of Pt ··· Pt separation and photophysics of binuclear platinum complexes. *J. Am. Chem. Soc.* **2005**, *127*, 28.

(14) Yu, C.; Chan, K. H.-Y.; Wong, K. M.-C.; Yam, V. W.-W. Single-stranded nucleic acid-induced helical self-assembly of alkynylplatinum(II) terpyridyl complexes. *Proc. Natl. Acad. Sci. U. S. A.* **2006**, *103*, 19652.

(15) Park, G.; Kim, H.; Yang, H.; Park, K. R.; Song, I.; Oh, J. H.; Kim, C.; You, Y. Amplified circularly polarized phosphorescence from co-assemblies of platinum(II) complexes. *Chem. Sci.* **2019**, *10*, 1294.

(16) Wan, Q.; To, W.-P.; Yang, C.; Che, C.-M. The metal−metal-to-ligand charge transfer excited state and supramolecular polymerization of luminescent pincer Pd^{II}-isocyanide complexes. *Angew. Chem., Int. Ed.* **2018**, *57*, 3089.

(17) Zou, C.; Lin, J.; Suo, S.; Xie, M.; Chang, X.; Lu, W. Palladium(II) N-heterocyclic allenylidene complexes with extended intercationic Pd···Pd interactions and MMLCT phosphorescence. *Chem. Commun.* **2018**, *54*, 5319.

(18) Chen, Y.; Li, K.; Lu, W.; Chui, S. S.-Y.; Ma, C.-W.; Che, C.-M. Photoresponsive supramolecular organometallic nanosheets induced by Pt^{II}···Pt^{II} and C-H··· π interactions. *Angew. Chem., Int. Ed.* **2009**, *48*, 9909.

(19) Yuen, M.-Y.; Roy, V. A. L.; Lu, W.; Kui, S. C. F.; Tong, G. S. M.; So, M.-H.; Chui, S. S.-Y.; Muccini, M.; Ning, J. Q.; Xu, S. J.;

Che, C.-M. Semiconducting and electroluminescent nanowires self-assembled from organoplatinum(II) complexes. *Angew. Chem., Int. Ed.* **2008**, *47*, 9895.

(20) Lu, W.; Roy, V. A. L.; Che, C.-M. Self-assembled nanostructures with tridentate cyclometalated platinum(II) complexes. *Chem. Commun.* **2006**, 3972.

(21) Aliprandi, A.; Mauro, M.; De Cola, L. Controlling and imaging biomimetic self-assembly. *Nat. Chem.* **2016**, *8*, 10.

(22) Wan, Q.; Xiao, X.-S.; To, W.-P.; Lu, W.; Chen, Y.; Low, K.-H.; Che, C.-M. Counteranion and solvent mediated chirality transfer in the supramolecular polymerization of luminescent platinum(II) complexes. *Angew. Chem., Int. Ed.* **2018**, *57*, 17189.

(23) Kemper, B.; Zengerling, L.; Spitzer, D.; Otter, R.; Bauer, T.; Besenius, P. Kinetically controlled stepwise self-assembly of Au^{I}-metallopeptides in water. *J. Am. Chem. Soc.* **2018**, *140*, 534.

(24) Würthner, F. Supramolecular polymerization: living it up. *Nat. Chem.* **2014**, *6*, 171.

(25) Ogi, S.; Stepanenko, V.; Thein, J.; Wuerthner, F. Impact of alkyl spacer length on aggregation pathways in kinetically controlled supramolecular polymerization. *J. Am. Chem. Soc.* **2016**, *138*, 670.

(26) Ma, X.; Zhang, Y.; Zhang, Y.; Liu, Y.; Che, Y.; Zhao, J. Fabrication of chiral-selective nanotubular heterojunctions through living supramolecular polymerization. *Angew. Chem., Int. Ed.* **2016**, *55*, 9539.

(27) Rao, K. V.; Miyajima, D.; Nihonyanagi, A.; Aida, T. Thermally bisignate supramolecular polymerization. *Nat. Chem.* **2017**, *9*, 1133.

(28) Korevaar, P. A.; George, S. J.; Markvoort, A. J.; Smulders, M. M. J.; Hilbers, P. A. J.; Schenning, A. P. H. J.; De Greef, T. F.; Meijer, E. W. Pathway complexity in supramolecular polymerization. *Nature* **2012**, *481*, 492.

(29) Jonkheijm, P.; van der Schoot, P.; Schenning, A. P. H. J.; Meijer, E. W. Probing the solvent-assisted nucleation pathway in chemical self-assembly. *Science* **2006**, *313*, 80.

(30) Zhang, W.; Jin, W.; Fukushima, T.; Saeki, A.; Seki, S.; Aida, T. Supramolecular linear heterojunction composed of graphite-like semiconducting nanotubular segments. *Science* **2011**, *334*, 340.

(31) Langenstroer, A.; Kartha, K. K.; Dorca, Y.; Droste, J.; Stepanenko, V.; Albuquerque, R. Q.; Hansen, M. R.; Sánchez, L.; Fernández, G. Unraveling concomitant packing polymorphism in metallosupramolecular polymers. *J. Am. Chem. Soc.* **2019**, *141*, 5192

(32) Endo, M.; Fukui, T.; Jung, S. H.; Yagai, S.; Takeuchi, M.; Sugiyasu, K. Photoregulated living supramolecular polymerization established by combining energy landscapes of photoisomerization and nucleation-elongation processes. *J. Am. Chem. Soc.* **2016**, *138*, 14347.

(33) Rupar, P. A.; Chabanne, L.; Winnik, M. A.; Manners, I. Non-centrosymmetric cylindrical micelles by unidirectional growth. *Science* **2012**, *337*, 559.

(34) Ogi, S.; Sugiyasu, K.; Manna, S.; Samitsu, S.; Takeuchi, M. Living supramolecular polymerization realized through a biomimetic approach. *Nat. Chem.* **2014**, *6*, 188.

(35) Wagner, W.; Wehner, M.; Stepanenko, V.; Ogi, S.; Würthner, F. Living supramolecular polymerization of a perylene bisimide dye into fluorescent J-aggregates. *Angew. Chem., Int. Ed.* **2017**, *56*, 16008.

(36) Kang, J.; Miyajima, D.; Mori, T.; Inoue, Y.; Itoh, Y.; Aida, T. A rational strategy for the realization of chain-growth supramolecular polymerization. *Science* **2015**, *347*, 646.

(37) Zhang, K.; Yeung, M. C.-L.; Leung, S. Y.-L.; Yam, V. W.-W. Living supramolecular polymerization achieved by collaborative assembly of platinum(II) complexes and block copolymers. *Proc. Natl. Acad. Sci. U. S. A.* **2017**, 201712827.

(38) Pal, A.; Malakoutikhah, M.; Leonetti, G.; Tezcan, M.; Colomb-Delsuc, M.; Nguyen, V. D.; van der Gucht, J.; Otto, S. Controlling the structure and length of self-synthesizing supramolecular polymers through nucleated growth and disassembly. *Angew. Chem., Int. Ed.* **2015**, *54*, 7852.

(39) Jin, X.-H.; Price, M. B.; Finnegan, J. R.; Boott, C. E.; Richter, J. M.; Rao, A.; Menke, S. M.; Friend, R. H.; Whittell, G. R.; Manners, I. Long-range exciton transport in conjugated polymer nanofibers prepared by seeded growth. *Science* **2018**, *360*, 897.

(40) Ogi, S.; Matsumoto, K.; Yamaguchi, S. Seeded polymerization through the interplay of folding and aggregation of an amino-acid-based diamide. *Angew. Chem., Int. Ed.* **2018**, *57*, 2339.

(41) Greciano, E. E.; Matarranz, B.; Sánchez, L. Pathway complexity versus hierarchical self-assembly in *N*-annulated perylenes: structural effects in seeded supramolecular polymerization. *Angew. Chem., Int. Ed.*. **2018**, *57*, 4697.

(42) Choi, I.; Yang, S.; Choi, T.-L. Preparing semiconducting nanoribbons with tunable length and width via crystallization-driven self-assembly of a simple conjugated homopolymer. *J. Am. Chem. Soc.* **2018**, *140*, 17218.

(43) Oosawa, F.; Kasai, M. A theory of linear and helical aggregations of macromolecules. *J. Mol. Biol.* **1962**, *4*, 10.

(44) Xi, J.; Xu, X. Understanding the anion-π interactions with tetraoxacalix[2]arene[2]triazine. *Phys. Chem. Chem. Phys.* **2016**, *18*, 6913.

(45) Xiao, X.-S.; Zou, C.; Guan, X.; Yang, C.; Lu, W.; Che, C.-M. Homoleptic gold(I) N-heterocyclic allenylidene complexes: excited-state properties and lyotropic chromonics. *Chem. Commun.* **2016**, *52*, 4983.

(46) Chow, P.-K.; To, W.-P.; Low, K.-H.; Che, C.-M. Luminescent palladium(II) complexes with π - extended cyclometalated [R-C^N^N-R'] and pentafluorophenylacetylide ligands: spectroscopic, photophysical, and photochemical properties. *Chem. - Asian J.* **2014**, *9*, 534.

(47) Leung, S. Y.-L.; Tam, A. Y.-Y.; Tao, C.-H.; Chow, H. S.; Yam, V. W.-W. Single-turn helix-coil strands stabilized by metal···metal and π - π interactions of the alkynylplatinum(II) terpyridyl moieties in *meta*-phenylene ethynylene foldamers. *J. Am. Chem. Soc.* **2012**, *134*, 1047.

(48) To, W.-P.; Tong, G. S. M.; Cheung, C.-W.; Yang, C.; Zhou, D.; Che, C.-M. Luminescent cyclometalated gold(III) alkyl complexes: photophysical and photochemical properties. *Inorg. Chem.* **2017**, *56*, 5046.

(49) Cheng, G.; Chan, K.-T.; To, W.-P.; Che, C.-M. Color tunable organic light-emitting devices with external quantum efficiency over 20% based on strongly luminescent gold(III) complexes having long-lived emissive excited states. *Adv. Mater.* **2014**, *26*, 2540.

(50) Tang, M.-C.; Lee, C.-H.; Lai, S.-L.; Ng, M.; Chan, M.-Y.; Yam, V. W.-W. Versatile design strategy for highly luminescent vacuum-evaporable and solution-processable tridentate gold(III) complexes with monoaryl auxiliary ligands and their applications for phosphorescent organic light emitting devices. *J. Am. Chem. Soc.* **2017**, *139*, 9341.

(51) To, W.-P.; Chan, K. T.; Tong, G. S. M.; Ma, C.; Kwok, W.-M.; Guan, X.; Low, K.-H.; Che, C.-M. Strongly luminescent gold(III) complexes with long-lived excited states: high emission quantum yields, energy up-conversion, and nonlinear optical properties. *Angew. Chem., Int. Ed.* **2013**, *52*, 6648.

(52) Pyykkö, P. Relativistic effects in chemistry: more common than you thought. *Annu. Rev. Phys. Chem.* **2012**, *63*, 45.

(53) Grimme, S.; Djukic, J.-P. cation−cation "attraction": when London dispersion attraction wins over Coulomb repulsion. *Inorg. Chem.* **2011**, *50*, 2619.

(54) Pyykkö, P. Relativistic effects in structural chemistry. *Chem. Rev.* **1988**, *88*, 563.

(55) Andrejić, M.; Mata, R. A. Study of ligand effects in aurophilic interactions using local correlation methods. *Phys. Chem. Chem. Phys.* **2013**, *15*, 18115.

(56) Weber, M.; Klein, J. E.; Miehlich, B.; Frey, W.; Peters, R. Monomeric ferrocene bis-imidazoline bis-palladacycles: variation of Pd-Pd distances by an interplay of metallophilic, dispersive, and coulombic interactions. *Organometallics* **2013**, *32*, 5810.

(57) Mann, K. R.; Gordon II, J. G.; Gray, H. B. Characterization of oligomers of tetrakis (phenyl isocyanide) rhodium(I) in acetonitrile solution. *J. Am. Chem. Soc.* **1975**, *97*, 3553.

(58) Oosawa, F.; Asakura, S. *Thermodynamics of the Polymerization of Protein*. Academic Press: London; New York, 1975.

(59) Zhao, D.; Moore, J. S. Nucleation-elongation: a mechanism for cooperative supramolecular polymerization. *Org. Biomol. Chem.* **2003**, *1*, 3471.

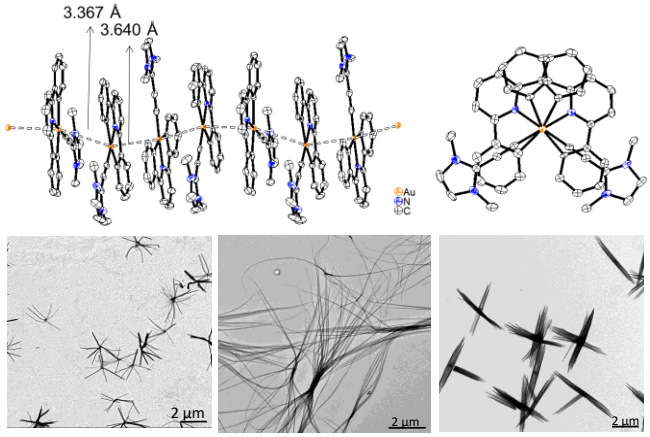
3.367 Å
3.640 Å
Au
N
C
2 µm
2 µm
2 µm